

# Quantum counterpart of Measure synchronization: A study on a pair of Harper systems

Saikat Sur<sup>a,\*</sup>, Anupam Ghosh<sup>a</sup>,

<sup>a</sup>*Department of Physics, Indian Institute of Technology Kanpur, Uttar Pradesh 208016, India*

## Abstract

Measure synchronization is a well-known phenomenon in coupled classical Hamiltonian systems over last two decades. In this paper, synchronization for coupled Harper system is investigated in both classical and quantum contexts. The concept of measure synchronization involves with the phase space and it seems that the measure synchronization is restricted in classical limit. But, on the contrary, here, we have extended the aforesaid synchronization in quantum domain. In quantum context, the coupling occurs between two many body systems via a time and site dependent potential. The coupling leads to the generation of entanglement between the quantum systems. We have used a technique, which is already accepted in the classical domain, in both the contexts to establish a connection between classical and quantum scenarios. Interestingly, results corresponding to both the cases lead to some common features.

**PACS numbers** 05.45.Xt, 05.45.-a, 03.65.Ud, 03.67.Bg,  
03.67.Hk, 75.10.Pq

**Keywords:** Measure synchronization, Coupled maps, Quantum Spin chains, Quantum correlations

## 1. Introduction

Synchronization was first observed in the seventeenth century by Huygens (Huygens, 1673), while working with the coupled pendulum clocks. Later, in the twentieth century, it was also reported that this phenomenon is observed in a triode generator, in two organ pipes, etc. (Pikovsky et al., 2001). In addition, the lighting of fireflies (Aguilar et al., 2011) is an example that supports the existence of this phenomenon in nature. Also, in the extended ecological systems (Blasius et al., 1999) and in the metabolic process (Porat-Shliom et al., 2014) we observe this phenomenon. However, much later, synchronization for the coupled chaotic systems was observed and chaotic synchronization becomes popular after 1990 (Pecora and Carroll, 1990).

Chaotic synchronization was challenging because of the sensitive dependence on the initial conditions. However, further progress in this field revealed the existence of the different kinds of synchronization, viz., phase synchronization, generalized synchronization, lag synchronization, etc. (Boccaletti et al., 2002). In delayed systems also, this phenomenon is observed (Pecora and Carroll, 2015). Though there is a vast literature for synchronization in coupled dissipative (Pecora and Carroll, 2015; Ghosh et al., 2018a) and coupled delay chaotic systems (Boccaletti et al., 2002), few articles are reported regarding the synchronization of Hamiltonian chaos. In the coupled Hamiltonian systems, the aforesaid synchronizations are

not observed. Also, since the Hamiltonian systems follow the Liouville's theorem, there is no existence of attractor here unlike the dissipative systems. Therefore, one would get a different type of synchronization: 'measure synchronization' (MS), in coupled Hamiltonian systems, reported in 1999 (Hampton and Zanette, 1999).

In case of MS, the participating subsystems share the same identical measure in the projected phase space (Hampton and Zanette, 1999). For two coupled Hamiltonian systems, if both the subsystems share the same area in the projected phase portraits, then the subsystems are in MS state, otherwise, not. Further, it is also reported that when there are more than two subsystems—say three subsystems—it may be observed that the first subsystem is in MS state with the third one, but not with the second one—this kind of synchronization is called the partial measure synchronization (Vincent, 2005). MS is studied in various branches of Physics, viz., in bosonic Josephson junction (Tian et al., 2013a), in delayed coupled Hamiltonian systems (Saxena et al., 2013), in ultra-cold atomic clouds (Qiu et al., 2015), in optomechanical systems (Bemani et al., 2017), etc.

Now, since synchronization in the coupled Hamiltonian systems is observed, one may extend the concept of the MS in the quantum systems. But, the first problem we face regarding this issue, is the fundamental idea behind the MS involves with the concept of the region covered by the phase space trajectory; there is no concept of phase space in quantum mechanics. However, recently, one article (Qiu et al., 2014) reported the quantum many body measure synchronization, and they have shown that both the coupling subsystems have identical measure in the

\*Corresponding author

Email addresses: saikatsu@iitk.ac.in (Saikat Sur),  
anupamgh@iitk.ac.in (Anupam Ghosh)

three dimensional angular momentum space. MS has also been studied in quantum many body systems (Qiu et al., 2010; Tian et al., 2013b) by extending the definition classical MS to quantum systems. Recently a study has been done on synchronization and quantum entanglement generation (Roulet and Bruder, 2018).

Quantum entanglement is a unique property of quantum mechanics. There is no analogue of entanglement in classical mechanics. Due to the linear superposition principle and tensorial structure in quantum mechanics, certain quantum state of two or more than two subsystems can not be written as a product of the states of individual subsystems. Hence, the subsystems can have quantum correlations even they are spatially separated. This results in certain phenomena which are exclusively quantum in nature (Einstein et al., 1935). Quantum entanglement has been studied in various contexts and recognized as an essential resource for quantum computation and information in last few decades.

Many body quantum systems specially quantum spins are of great interest in quantum communication theory as they could be used as quantum wires to join quantum devices. So quantum entanglement has also been extensively studied in the field of communication in quantum spin systems, viz., state transfer, entanglement transfer in quantum spin chains (Bose, 2003; Subrahmanyam, 2004; Christandl et al., 2004), etc. To establish a connection between the MS and the entanglement generation in many-body quantum systems, one needs to have a quantum system which behaves as a classical system showing measure synchronization in certain limit. Previously some studies show the connection between entanglement generation in higher dimensional quantum systems and chaos in their classical map (Lakshminarayan, 2001).

Here, we concentrate on a one dimensional periodically kicked Harper model with  $N$  qubits, i.e.,  $2^N$  dimensional Hilbert space. This model reduces to a classical Harper map for large  $N$  limit. This is an approximate model for electrons in a crystal lattice subjected to a perpendicular magnetic field (Harper, 1955). The dynamics of Bloch electrons moving in periodic potential in presence of a uniform magnetic field and time varying electric field can be shown to be governed by Harper dynamics under the tight binding approximation (Iomin and Fishman, 1998, 2000). The model has a rich spectral structure, and also relevant in the context of metal-insulator transition or transition from localized to extended states (Basu et al., 1991; Artuso et al., 1994, 1992). In addition, the quantum kicked Harper model has been investigated for the entanglement distribution and dynamics (Lakshminarayan and Subrahmanyam, 2003).

Since there is no closed form solution for the quantum model due to the space dependent on site potential we restrict ourselves in one particle subspace. However, it is possible to write time dependent wave-function for one particle states in analytical form as discussed in (Sur and Subrahmanyam, 2019). Coupling such two  $N$  qubit systems via another time and space dependent potential can result in interesting consequences. This leads to decoherence in individual systems and both the systems get correlated. Due to the absence of phase space in quantum mechanics, their coupling dynamics can be investigated by

studying their quantum correlation measures as well as intra qubit correlations from the two systems.

In this paper, we study the coupled Harper systems and try to observe the measure synchronization here. Since the concept of MS is purely classical, we try to study the coupled Harper systems in the classical limit. Further, we show that one can extend the idea of MS in the domain of coupled quantum systems. Thus, this manuscript aims to connect two completely different branches of physics, synchronization in chaotic systems and quantum many-body physics and intrigues some new avenues for further research. The manuscript is prepared in the following order: In section III, we explain the MS explicitly in the classical scenario, then we return to the quantum picture and study the dynamics in detailed in section IV, and try make an analogy. Finally, a short discussion on local coupling in quantum scenario has been added.

## 2. Preliminaries

We consider the following integrable Hamiltonian (Lakshminarayan and Subrahmanyam, 2003) of a one dimensional  $N$  body quantum system of fermions hopping on a chain with an inhomogeneous site potential. The Hamiltonian is given by:

$$H = \frac{1}{2} \sum_{j=1}^N c_j^\dagger c_{j+1} + \frac{g}{2} \sum_{j=1}^N d_j^\dagger d_{j+1} + \text{H.C.}, \quad (1)$$

where  $c_j^\dagger$  are the creation operators at site  $j$ ,  $g$  is the potential strength parameter. The operators  $d_k$  are the Fourier transformation of the Fermion annihilation operators and are given as follows:

$$d_k = \frac{1}{\sqrt{N}} \sum_{j=1}^N e^{\frac{2\pi ijk}{N}} c_j. \quad (2)$$

Substituting it in the actual Hamiltonian we get:

$$H = \sum_{j=1}^N \left[ \frac{1}{2} (c_j^\dagger c_{j+1} + c_j c_{j+1}^\dagger) + g \cos\left(\frac{2\pi j}{N}\right) c_j^\dagger c_j \right]. \quad (3)$$

Further, we denote the sum of the operators in the following way:

$$V = \sum_{j=1}^N c_{j+1}^\dagger c_j, \\ U = \sum_{k=1}^N d_k^\dagger d_{k+1} = \sum_{j=1}^N e^{\frac{2\pi ij}{N}} c_j^\dagger c_j, \quad (4)$$

and, it can be shown that the operators  $V$  and  $U$  are the discrete versions of standard quantum position and momentum translation operators:  $\exp(-ipa/\hbar)$  and  $\exp(-ixb/\hbar)$  respectively. Here,  $a$  and  $b$  are respectively the smallest position and the momentum units. A detailed explanation is given in (Lakshminarayan and Subrahmanyam, 2003). However, in terms of this new notation the Hamiltonian can be written as:

$$H = \frac{1}{2} [V + V^\dagger] + \frac{g}{2} [U + U^\dagger] \\ = \frac{1}{2} [V + V^\dagger] + \frac{g}{2} \sum_{j=1}^N \cos\left(\frac{2\pi j}{N}\right) c_j^\dagger c_j, \quad (5)$$

Now, we consider the non-integrable Hamiltonian, i.e., the second term on the right hand side of Eq. 5—which can also be thought of as a time dependent and site dependent potential term. The non-integrable Hamiltonian is given as:

$$\begin{aligned} H(t) &= \frac{1}{2}[V + V^\dagger] + \frac{g}{2}[U + U^\dagger] \sum_{n=-\infty}^{\infty} \delta(\frac{2\pi t}{\tau} - n) \\ &= \sum_{j=1}^N [\frac{1}{2}(c_j^\dagger c_{j+1} + c_j c_{j+1}^\dagger) + g \cos(\frac{2\pi j}{N}) c_j^\dagger c_j] \\ &\quad \sum_{n=-\infty}^{\infty} \delta(\frac{2\pi t}{\tau} - n). \end{aligned} \quad (6)$$

A train of impulses is provided at intervals of time  $\tau/(2\pi)$ , where  $\tau$  is the kicking interval parameter. As  $\tau \rightarrow 0$ , we recover the integrable Harper equations. The first term represents the kinetic energy of the fermion or hopping term, and the second term is the kicked potential energy operator. The effect of the potential is through a train of kicking pulses with an interval  $\tau$ , a tunable parameter, to go continuously from completely integrable to completely non-integrable regimes. For  $\tau \rightarrow 0$  the dynamics of the Harper Hamiltonian is integrable, and for large values of  $\tau$  the dynamics is completely chaotic (see Fig. 4 in the work of Lakshminarayan and Subrahmanyam (Lakshminarayan and Subrahmanyam, 2003), and for further details (Lima and Shepelyansky, 1991)). The potential strength parameter  $g$  and the kicking interval parameter  $\tau$  can be varied independently to change the dynamics qualitatively.

The Hilbert space for a single site is two-dimensional, either occupied or unoccupied, and thus it can be mapped to the spin language. We convert the Hamiltonian in Eq. 6 from fermion operator to spin operator formalism via Jordan-Wigner transformation (Lieb et al., 1961), where the fermion occupation is mapped to the down spin occupation in the spin states. The Hamiltonian can be written in terms of spin operator language as the following,

$$\begin{aligned} H(t) &= \sum_{j=1}^N [\frac{1}{4}[(\sigma_j^x \sigma_{j+1}^x + \sigma_j^y \sigma_{j+1}^y) \\ &+ g \cos(\frac{2\pi j}{N}) \frac{\sigma_j^z + 1}{2} \sum_{n=-\infty}^{\infty} \delta(\frac{2\pi t}{\tau} - n)]. \end{aligned} \quad (7)$$

The first term turns out to be XY term, and the second term becomes a transverse field that is inhomogeneous in space. This incorporates an interaction of down spins on neighbouring sites and there is no many-body interaction here.

Now, we discuss the coupling scheme of two identical Harper systems, denoted by  $A$  and  $B$  respectively, each with  $N$  particles, The time dependent coupling Hamiltonian is proposed by taking the product of potential terms from individual Hamiltonians. This coupling scheme is very much similar to (Miller and Sarkar, 1999). The time dependent Hamiltonian for the coupling term are given by the following,

$$H^{AB}(t) = \frac{\varepsilon}{2}[U^A + U^{A^\dagger}][U^B + U^{B^\dagger}] \sum_{n=-\infty}^{\infty} \delta(\frac{2\pi t}{\tau} - n), \quad (8)$$

where  $\varepsilon$  is the coupling strength parameter. The coupling strength parameter  $\varepsilon$  should be of same order of the potential strength parameter  $g$ . We set  $g$  unity throughout the paper and varied  $\varepsilon$  to see the measure Synchronization.

Using the definition for the operator  $U$  given in Eq. 4, we can write the coupling Hamiltonian in terms of the spin operators,

$$\begin{aligned} H^{AB}(t) &= \frac{\varepsilon}{2} \sum_{j_A, j_B=1}^N \cos(\frac{2\pi j_A}{N}) \cos(\frac{2\pi j_B}{N}) \sigma_{j_A}^z \sigma_{j_B}^z \\ &\quad \sum_{n=-\infty}^{\infty} \delta(\frac{2\pi t}{\tau} - n). \end{aligned} \quad (9)$$

Rest of the terms vanish because of the transverse potential being symmetric in site, i.e.,  $\sum_{j=1}^N \cos(\frac{2\pi j}{N}) = 0$ . Though there is no many body interactions in each of the systems, but coupling introduces an inter system many body interaction effect. This will generate inter-system correlation along with intra-system correlation. We can construct the full Hamiltonian that governs the the dynamics of the joint quantum system from Eq. 7 and Eq. 8 as the following,

$$\begin{aligned} H(t) &= \frac{1}{4}(\sum_{j_A=1}^N (\sigma_{j_A}^x \sigma_{j_A+1}^x + \sigma_{j_A}^y \sigma_{j_A+1}^y) \\ &+ \sum_{j_B=1}^N (\sigma_{j_B}^x \sigma_{j_B+1}^x + \sigma_{j_B}^y \sigma_{j_B+1}^y)) \\ &+ \frac{1}{2}(g \sum_{j_A=1}^N \cos(\frac{2\pi j_A}{N}) \sigma_{j_A}^z + g \sum_{j_B=1}^N \cos(\frac{2\pi j_B}{N}) \sigma_{j_B}^z \\ &+ \varepsilon \sum_{j_A, j_B=1}^N \cos(\frac{2\pi j_A}{N}) \cos(\frac{2\pi j_B}{N}) \sigma_{j_A}^z \sigma_{j_B}^z) \sum_{n=-\infty}^{\infty} \delta(\frac{2\pi t}{\tau} - n). \end{aligned} \quad (10)$$

The operators  $U$  and  $V$  we introduced in Eq. 4 are lattice translation and momentum translation operators respectively, and this can easily seen as:

$$V|l\rangle = |l+1\rangle, \quad \langle k|U = \langle k+1|. \quad (11)$$

If we replace  $V$  and  $U$  by discrete versions of standard quantum position and momentum translation operators  $\exp(-ipa/\hbar)$  and  $\exp(-ixb/\hbar)$  respectively Eq. 6 leads to,

$$H(t) = \cos(\frac{pa}{\hbar}) + g \cos(\frac{xb}{\hbar}) \sum_{n=-\infty}^{\infty} \delta(\frac{2\pi t}{\tau} - n) \quad (12)$$

Setting  $a = b = 1/N$ ,  $\hbar = 1/2\pi N$ , and replacing the operators  $x$  and  $p$  by their classical values  $x$  and  $p$  respectively, the classical Harper Hamiltonian can be obtained as,

$$H_c(t) = \cos(2\pi p) + g \cos(2\pi x) \sum_{n=-\infty}^{\infty} \delta(\frac{2\pi t}{\tau} - n), \quad (13)$$

where the subscript ‘c’ abbreviates the classical counterpart of the Hamiltonian. Similarly, the classical coupling Hamiltonian in Eq. 8 turns out to be,

$$H_c^{AB}(t) = 2\varepsilon \cos(2\pi x^A) \cos(2\pi x^B) \sum_{n=-\infty}^{\infty} \delta(\frac{2\pi t}{\tau} - n). \quad (14)$$

The dynamics of the full system is governed by the Hamiltonians  $H^A(t)$ ,  $H^B(t)$  of the subsystems  $A$  and  $B$  and the interacting term  $H^{AB}(t)$ . The full Hamiltonian  $H_c(t)$  is given by,

$$\begin{aligned} H_c(t) &= H_c^A(t) + H_c^B(t) + H_c^{AB}(t) \\ &= \cos(2\pi p^A) + \cos(2\pi p^B) + g(\cos(2\pi x^A) + g \cos(2\pi x^B) \\ &+ 2\varepsilon \cos(2\pi x^A) \cos(2\pi x^B)) \sum_{n=-\infty}^{\infty} \delta(\frac{2\pi t}{\tau} - n). \end{aligned} \quad (15)$$

### 3. Observation of measure synchronization

Now, since we have the Hamiltonian in the classical limit, we want to study here the dynamics of two coupled Harper systems and try to observe whether we have some analogous results in the quantum scenario. Since  $\tau$  is the time interval between two consecutive kicks, then time  $t = n\tau$ , where  $n$  is an integer. Following (Lakshminarayan and Subrahmanyam, 2003), the equation of motions of the coupled systems become:

$$x^A(n+1) = x^A(n) - \tau \sin(2\pi p^A(n)), \quad (16a)$$

$$p^A(n+1) = p^A(n) + \tau g \sin(2\pi x^A(n+1)) + 2\tau \varepsilon \sin(2\pi x^A(n)) \cos(2\pi x^B(n)), \quad (16b)$$

$$x^B(n+1) = x^B(n) - \tau \sin(2\pi p^B(n)), \quad (16c)$$

$$p^B(n+1) = p^B(n) + \tau g \sin(2\pi x^B(n+1)) + 2\tau \varepsilon \sin(2\pi x^B(n)) \cos(2\pi x^A(n)). \quad (16d)$$

The newly constructed maps (Eq. 16) are defined within 0 and 1 using the standard ‘mod’ function (Lakshminarayan and Subrahmanyam, 2003). The dynamics of the individual system (i.e., with  $H_c^{AB} = 0$ ) is already studied for different  $\tau$  in (Lakshminarayan and Subrahmanyam, 2003). The individual system (i.e., either  $H_c^A$  or  $H_c^B$  with  $H_c^{AB} = 0$ ) shows non-chaotic and chaotic motions at  $\tau = 0.1$  and  $\tau = 0.5$  respectively, and a mixed state of chaotic and non-chaotic dynamics is observed at  $\tau = 0.3$  (Lakshminarayan and Subrahmanyam, 2003). However, in this paper, we study the measure synchronization (Hampton and Zanette, 1999) the coupled systems (i.e., with  $H_c^{AB} \neq 0$ ) at different values of  $\tau$ . In the case of coupled Hamiltonian systems, we generally observed measure synchronization (Hampton and Zanette, 1999; Wang et al., 2002, 2003; Vincent, 2005; Gupta et al., 2017), which imply that in synchronized state the coupled systems share the identical regions (or, area) of the projected phase space—hence the name ‘measure’. In literature, there are two techniques, viz., equal average energy of participating systems (Wang et al., 2003; Vincent, 2005) and kink in average interaction energy (Wang et al., 2003) to detect the measure synchronized state. But, recently, two works (Gupta et al., 2017; Ghosh et al., 2018b) reported that sometimes the equal bare energy technique fails to detect the synchronized state and encourage to use the other technique: kink in average interaction energy. Anyway, one can always back to the first principle of measure synchronization and compare the joint probability density functions of the coupled systems for the verification of the synchronized state (Ghosh et al., 2018b). However, for the further analysis, we adopt the joint probability density technique and the average interaction energy method to illustrate our results. From now onwards we use the term ‘synchronization’ to refer the measure synchronization.

#### 3.1. Joint probability density technique

In Fig. 1, we have studied the  $\tau = 0.3$  case in detailed in presence of two different values coupling strengths  $\varepsilon : 0.3$  (a and b) and  $0.7$  (c and d), and observe that two coupled oscillators are not in the synchronized state at  $\varepsilon = 0.3$ , but in synchrony at

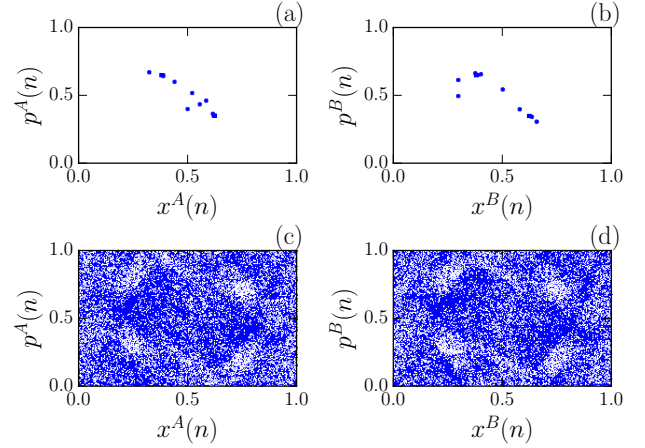


Figure 1: Measure desynchronization and measure synchronization are observed for different coupling strengths. The phase portraits of the individual subsystems, following Eq. 16, are plotted for two different values of coupling strength  $\varepsilon$  keeping fixed  $\tau = 0.3$  and  $g = 1$  in both the cases. First row (a and b) is for  $\varepsilon = 0.3$ , whereas the last row (c and d) is for  $\varepsilon = 0.7$ . For  $\varepsilon = 0.7$ , both the subsystems are in synchronized state unlike the scenario at  $\varepsilon = 0.3$ . In both the subplots, we have taken the initial condition as  $(x^A(0), p^A(0), x^B(0), p^B(0)) = (0.5, 0.4, 0.3, 0.5)$ .

$\varepsilon = 0.7$ . Thus, the visual observation is a qualitative support of the synchronized state at  $\varepsilon = 0.7$ . Now before comparing the joint probability distribution function, let us briefly discuss the algorithm to calculate the joint probability distribution in the next paragraph.

The phase portrait of either system is bounded within 0 and 1—both in abscissa and ordinate. Let us divide the projected phase portrait—the  $x^A - p^A$  plane (or, the  $x^B - p^B$  plane)—into small square of area  $\Delta x \Delta p = 1/M^2$ , i.e., we divide either of the axes into  $M$  small pieces with  $\Delta x := 1/M$  and  $\Delta p := 1/M$ . Thus,  $\rho^A(x^A, p^A) \Delta x \Delta p$  provides the fraction of total points within a square of area  $\Delta x \Delta p$  with centre at  $(x^A, p^A)$ , where  $\rho^A(x^A, p^A)$  is the joint probability distribution of the subsystem  $A$ . Similarly, we can define the joint probability distribution function— $\rho^B(x^B, p^B)$ —of the second subsystem  $B$ . Now, the coupled subsystems are in measure synchronized state if  $\Delta \rho := |\rho^A(x, p) - \rho^B(x, p)| \leq \rho_c \forall (x, p)$ , where  $\rho_c$  is a threshold and should be infinitesimally small.

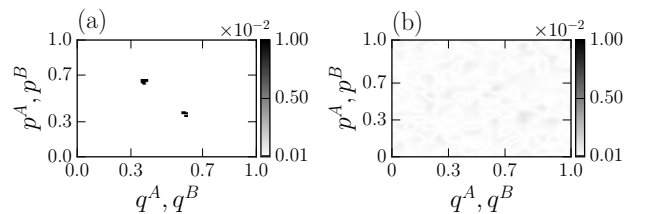


Figure 2: Fig. 1 is depicted here from a quantitative point of view: comparing the joint probability densities of the coupling subsystems.  $\Delta \rho$  is plotted in colour in (a) and (b) for  $\varepsilon = 0.3$  and  $0.7$  respectively. In (a),  $\Delta \rho$  is larger than the threshold  $\rho_c (= 1 \times 10^{-3})$ , indicating the desynchronized state. But in (b), the condition  $\Delta \rho \leq \rho_c$  is always satisfied indicating the synchronized state.

In theory,  $\rho_c$  should be zero. However, this demands that

the time-series under study be infinitely long and be sampled continuously in time. In practice, this is impossible. Hence, the best we can do is to choose  $\rho_c$  to be some small non-zero number depending on how long the systems are evolved in the numerical simulations. We have taken  $M = 20$ , i.e., the joint probability distribution is calculated over total  $20 \times 20$  grids, and the threshold  $\rho_c$  is taken as  $1 \times 10^{-3}$ . Note that there is nothing special about  $M = 20$ . One may choose any larger  $M$ . The choice of smaller values of  $M$  has the obvious problem that the information of the local dynamics can't be captured—as an extreme example,  $M = 1$  can only capture an averaged global measure. Also, in practice,  $\rho_c$  depends on the  $M$  value—this dependence would also vanish in the limit of infinitely long data that has been sampled continuously.

### 3.2. Average interaction energy technique

As discussed at the beginning of this section, the average interaction energy indicate the transition from a synchronized state to desynchronized state or vice versa. Here, the average interaction energy of the coupled subsystems ( $A$  and  $B$ ), following Eq. 15, is given by:

$$E^{\text{int}} = \frac{1}{T} \sum_{n=1}^T H_c^{AB}(n). \quad (17)$$

In addition with the phase coordinates,  $E^{\text{int}}$  depends explicitly on the the coupling strength. The average interaction energy is plotted in Fig. 3(a) with different  $\varepsilon$  using Eq. 16 and 17. One kink is observed at  $\varepsilon = 0.5$ , which further implies that there is a transition from the desynchronized state to the synchronized state at  $\varepsilon = 0.5$  (Gupta et al., 2017) as  $\varepsilon$  is increased. For more clear understanding, we have plotted the phase portraits at  $\varepsilon = 0.3$  and  $0.7$  in Fig. 1. Fig. 1 leads to the conclusion that at  $\varepsilon = 0.3$ , the participating subsystems are in desynchronized state, whereas at  $\varepsilon = 0.7$  they occupy the same measure in the projected phase space indicating the synchronized state.

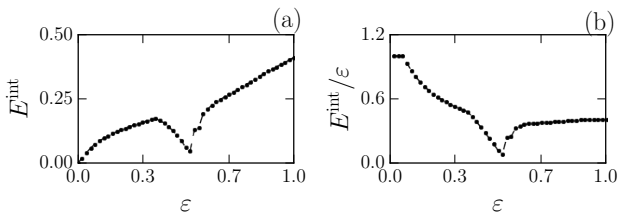


Figure 3: The average interaction energy  $E^{\text{int}}$  is plotted for the coupled subsystems  $A$  and  $B$  following Eq. 16 and 17 for different coupling strengths  $\varepsilon$  with the initial condition  $(x^A(0), p^A(0), x^B(0), p^B(0)) = (0.5, 0.4, 0.3, 0.5)$ . A kink observed at  $\varepsilon = 0.5$  shows the transition from the desynchronized state to the synchronized state.

Thus we may conclude here, with the help of above mentioned techniques, that synchronized state is observed for coupled Harper systems after  $\varepsilon = 0.5$  using  $\tau = 0.3$ . However, the scenario is different for other values of  $\tau$ . For example, if we choose  $\tau = 0.1$ , we observe a discontinuity in  $E^{\text{int}}$  at  $\varepsilon = 0.5$  (see Fig. 4(a) or (b)), and following our discussion there should

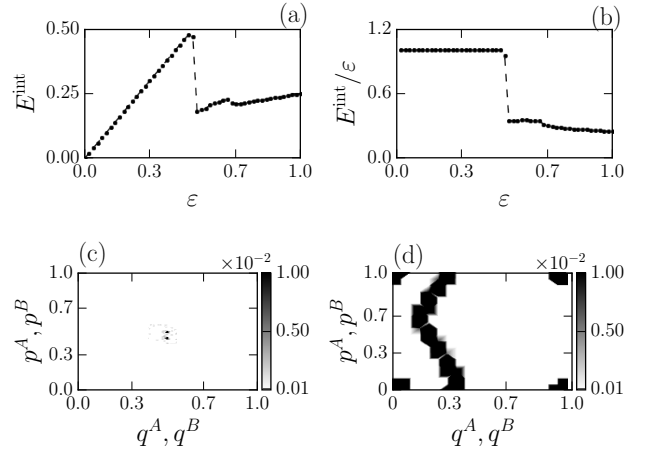


Figure 4: Similar to Fig. 3 and 2,  $E^{\text{int}}$  and  $\Delta\rho$  are plotted for the coupled subsystems  $A$  and  $B$  for different coupling strengths  $\varepsilon$  with  $\tau = 0.1$  and unaltered initial conditions  $(x^A(0), p^A(0), x^B(0), p^B(0)) = (0.5, 0.4, 0.3, 0.5)$ . A discontinuity observed at  $\varepsilon = 0.5$ , but no transition is observed at  $\varepsilon = 0.5$ . Subplots (c) and (d) show the variation of  $\Delta\rho$  for  $\varepsilon = 0.3$  and  $0.7$  respectively. The higher values of  $\Delta\rho$  ( $\Delta\rho > \rho_c$  with  $\rho_c = 4 \times 10^{-4}$ ) imply the desynchronized state in both the cases.

be a transition between the desynchronized and the synchronized state. But, the variation of  $\Delta\rho$  (see Fig. 4(c) or (d)) explain that for both the cases:  $\varepsilon = 0.3$  and  $0.7$ , desynchronized state is observed. Thus, the discontinuity in  $E^{\text{int}}$ , observed here, misguided us to make a decision, and the aforesaid problem continued for all values of  $\tau \lesssim 0.3$ . Besides, for  $\tau \gtrsim 0.3$ , we do not observe the transition for any  $\varepsilon \in [0, 1]$ . In Fig. 5 we have explained the case for  $\tau = 0.5$  and no kink is observed in  $E^{\text{int}}$  (see Fig. 5(a) or (b)), which maybe because of the full-fledged chaotic nature of the coupled subsystems at  $\tau = 0.5$  (Lakshminarayan and Subrahmanyam, 2003; Lima and Shepelyansky, 1991) and they are always in synchronized state. The values of  $\Delta\rho$  in Fig. 5(c) or (d) support the existence of the synchronized states for  $\text{varepsilonpsilon} = 0.3$  and  $0.7$ . This further help us to make a possible conclusion that *the transition is always associated with a kink in  $E^{\text{int}}$ , but any non-analyticity in  $E^{\text{int}}$  does not imply the transition*. However, all the conclusions drawn from the results in this section remain unchanged from other sets of initial conditions also.

## 4. Quantum Dynamics

Now, we turn our discussions on time evolution of quantum systems  $A$  and  $B$ , and each of the systems is an  $N$  qubit system. The operators in the systems  $A$  and  $B$  belong to disjoint Hilbert spaces  $\mathbb{H}^A$  and  $\mathbb{H}^B$  respectively. Even initially each of the system starts from a pure state, due to the coupling eventually they will entangle with each other and become mixed states hence we have to evolve both the systems simultaneously. Let  $|\psi_0^A\rangle$  and  $|\psi_0^B\rangle$  be the initial states of systems  $A$  and  $B$  respectively. The state of the joint system can be written as  $|\psi_0\rangle = |\psi_0^A\rangle \otimes |\psi_0^B\rangle$ . We consider evolution at discrete times, viz.,  $t = \tau^+ / 2\pi, 2\tau^+ / 2\pi$ , etc., i.e., at time instant just after a kick. The

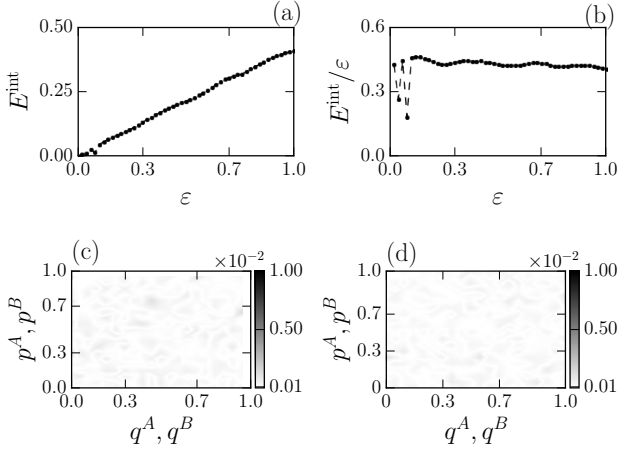


Figure 5: This plot is for  $\tau = 0.5$  with the initial condition  $(x^A(0), p^A(0), x^B(0), p^B(0)) = (0.5, 0.4, 0.3, 0.5)$ . Here no kink is observed in  $E^{\text{int}}$  for different coupling strengths  $\epsilon$ , which supports the absence of the transition. The density plots of  $\Delta\rho$ , for  $\epsilon = 0.3$  (subplot (c)) and  $0.7$  (subplot (d)), are also in accordance with this conclusion.

state of the joint system after  $n$  kicks will be given by:

$$|\psi_{n\tau/2\pi}\rangle = \mathcal{U}^n |\psi_0\rangle = \mathcal{U}^n |\psi_0^A\rangle \otimes |\psi_0^B\rangle, \quad (18)$$

where, the time evolution operator  $\mathcal{U}$  is defined on the joint Hilbert space  $\mathbb{H}^A \otimes \mathbb{H}^B$  just for one kick (corresponding to  $t = \tau/2\pi$ ).

To solve the system analytically, we need to focus on the symmetry of the dynamics. It can be easily seen that number of down spins is conserved throughout the dynamics in the joint system as well as in the individual systems. The XY dynamics can be studied analytically using Bethe Ansatz eigenfunctions (Bethe, 1931). The one-magnon excitations can be created by turning any one of the spins, giving  $N$  localized one-magnon states. One-magnon eigenstates are labelled by the momentum of the down spin and the corresponding eigenfunction is given by:

$$\phi_p^x = \sqrt{\frac{1}{N}} e^{ipx}; p = \frac{2\pi l}{N}, \text{ for a closed chain,} \quad (19)$$

where the momentum  $p$  is determined by an integer  $l = 1, 2, \dots, N$ . The one-magnon eigenvalue is given by  $\epsilon_1(p) = -\cos p$ . The time evolution of the system will transport the single down spin from site  $x$  to another site  $x'$  and the time dependent probability is given by one magnon Green function, where the time-dependent function  $G_x^{x'}(t)$  (Subrahmanyam, 2004; Sur and Subrahmanyam, 2017) is given by:

$$G_x^{x'}(t) = (-i)^{x-x'} J_{x-x'}(t), \quad (20)$$

for a closed chain.  $J_x(y)$  is the Bessel function of integer order  $x$  and argument  $y$ . The system evolves between a time  $n\tau/2\pi$  to  $(n+1)\tau/2\pi$  through XY dynamics between two kicks which introduces a lattice position dependent phase factor to the Green function (Sur and Subrahmanyam, 2019). It can be seen that after each kick, a site-dependent new phase is introduced in the Green function which indicates the qualitative change in the

dynamics from XY dynamics, i.e., the state after a kick depends on the location of the down spin after the previous kick.

The most general initial state to start the dynamics with is  $M_A$  number of down spins in system  $A$  and  $M_B$  number of down spins in system  $B$ . The most trivial state to start the dynamics is where there is no down spin in one of the systems. But for such initial state the systems will not get correlated through the coupling. Since no bound state is formed even for multiple number of down spins in the individual systems, the wave function for any general initial state can be obtained from the product of non-interacting one particle Green functions. So, no new physics is coming out for any multimagnon state as the initial state. But to observe the transition, it is necessary that the individual systems start with different initial states. Since we have discussed that the dynamics is qualitatively independent of the initial conditions, any initial states is sufficient to observe the transition. Hence, we restrict ourselves to one particle initial states ( $M_A = 1$  and  $M_B = 1$ , i.e., a direct-product state with  $1 + 1$  number of down spins) for simplicity of calculations. The initial state is denoted as:

$$|\psi_0\rangle = |x_0; y_0\rangle, \quad (21)$$

where  $x_0(y_0)$  denotes the location of the down spin in system  $A(B)$ .  $x_i$  are the co-ordinates of the sites with down spins in system  $A$  after  $i^{\text{th}}$  kick, and similarly,  $y_i$  are for system  $B$ .

We show the time evolution of the state explicitly for one kick. The time evolution operator  $\mathcal{U}$  acting on the the state  $|x_0; y_0\rangle$  yields the following state at time  $t = \tau/2\pi$ ,

$$\begin{aligned} |\psi_{t=\tau/2\pi}\rangle &= \mathcal{U} |x_0; y_0\rangle \\ &= e^{\frac{i}{2}g(\sum_{j_A=1}^N \cos(\frac{2\pi j_A}{N})\sigma_{j_A}^z + \sum_{j_B=1}^N \cos(\frac{2\pi j_B}{N})\sigma_{j_B}^z)} \\ &\quad \times e^{\frac{i}{2}\epsilon \sum_{j_A, j_B=1}^N \cos(\frac{2\pi j_A}{N}) \cos(\frac{2\pi j_B}{N}) \sigma_{j_A}^x \sigma_{j_B}^x} \\ &\quad \times e^{\frac{i\tau}{4}(\sum_{j_A=1}^N (\sigma_{j_A}^x \sigma_{j_{A+1}}^x + \sigma_{j_A}^y \sigma_{j_{A+1}}^y) + \sum_{j_B=1}^N (\sigma_{j_B}^x \sigma_{j_{B+1}}^x + \sigma_{j_B}^y \sigma_{j_{B+1}}^y))} |x_0; y_0\rangle \\ &= \sum_{x_1, y_1} G_{x_0}^{x_1}(\frac{\tau}{2\pi}) G_{y_0}^{y_1}(\frac{\tau}{2\pi}) e^{i(g \cos(\frac{2\pi x_1}{N}) + g \cos(\frac{2\pi y_1}{N}) - 2\epsilon \cos(\frac{2\pi x_1}{N}) \cos(\frac{2\pi y_1}{N}))} |x_1; y_1\rangle \end{aligned} \quad (22)$$

Extending Eq. 22 by recursion relation for  $n$  kicks the joint quantum state at time  $t = n\tau/2\pi$  is given in following form :

$$|\psi_{t=n\tau/2\pi}\rangle = \sum_{x_n, y_n} \tilde{G}_{x_0, y_0}^{x_n, y_n}(n) |x_n; y_n\rangle, \quad (23)$$

where the wave function  $\tilde{G}_{x_0, y_0}^{x_n, y_n}(n)$  in the above equation is the Green function of the coupled joint system and given in terms of one magnon Green functions as:

$$\begin{aligned} \tilde{G}_{x_0, y_0}^{x_n, y_n}(n) &= \sum_{x_1, x_2, \dots, x_{n-1}} \sum_{y_1, y_2, \dots, y_{n-1}} \prod_{i=0}^{n-1} G_{x_i}^{x_{i+1}}(\frac{\tau}{2\pi}) G_{y_i}^{y_{i+1}}(\frac{\tau}{2\pi}) \\ &\quad \times e^{i(g \cos(\frac{2\pi x_{i+1}}{N}) + g \cos(\frac{2\pi y_{i+1}}{N}) - 2\epsilon \cos(\frac{2\pi x_{i+1}}{N}) \cos(\frac{2\pi y_{i+1}}{N}))}. \end{aligned} \quad (24)$$

Energies of the individuals systems  $A$  and  $B$  as well as the interaction energy can be computed from the above wave function. Energies  $E^A$  and  $E^B$  of the systems  $A$  and  $B$  respectively after  $n$  kicks are given by,

$$\begin{aligned}
E_n^A &= \frac{1}{2} \sum_{x_n, y_n} \tilde{G}_{x_0, y_0}^{*x_n, y_n}(n) (\tilde{G}_{x_0, y_0}^{x_n+1, y_n}(n) + \tilde{G}_{x_0, y_0}^{x_n-1, y_n}(n)); \\
E_n^B &= \frac{1}{2} \sum_{x_n, y_n} \tilde{G}_{x_0, y_0}^{*x_n, y_n}(n) (\tilde{G}_{x_0, y_0}^{x_n, y_n+1}(n) + \tilde{G}_{x_0, y_0}^{x_n, y_n-1}(n)).
\end{aligned} \tag{25}$$

The interaction energy after  $n$  kicks is given by,

$$\begin{aligned}
E_n^{\text{int}} &= \sum_{x_n, y_n} |\tilde{G}_{x_0, y_0}^{x_n, y_n}(n)|^2 \langle x_n, y_n | H^{AB} | x_n, y_n \rangle \\
&= 2\varepsilon \sum_{x_n, y_n} |\tilde{G}_{x_0, y_0}^{x_n, y_n}(n)|^2 \cos\left(\frac{2\pi x_n}{N}\right) \cos\left(\frac{2\pi y_n}{N}\right).
\end{aligned} \tag{26}$$

Unlike the classical scheme, where the interaction takes place only between two systems through the coupling, the quantum counterpart is more complicated. Here, the individual systems ( $A$  and  $B$ ) as well as individual qubits in each systems though uncorrelated initially, will generate multi party correlation through time evolution.  $N$  qubits in system  $A$  will get correlated with  $N$  qubits in system  $B$ , this is a multi party correlation. Also each qubit in system  $A$  (or  $B$ ) will get correlated with the rest ( $N - 1$ ) qubits in system  $A$  (or  $B$ ) as well as  $N$  qubits of system  $B$  (or  $A$ ). The correlation between system  $A$  and  $B$  is quantified through the reduced density matrix (RDM) of the systems. Since we know the joint state at any time  $t$ , the RDM for any system can be computed by tracing out the rest from the joint density matrix. The definition of the RDM for any subsystem  $X$  is given by,

$$\rho^X = \text{Tr}_{\bar{X}} |\psi\rangle\langle\psi|, \tag{27}$$

where,  $\text{Tr}_{\bar{X}}$  is the partial trace over the Hilbert space excluding the subsystem  $X$ . All informational based correlation measures are computed from the RDM, e.g., the von Neumann entropy of the subsystem  $A$  will be given as,

$$S_t^A = -\text{Tr} \rho_t^A \ln \rho_t^A. \tag{28}$$

The von Neumann entropy  $S_t^A$  measures entanglement between the system  $A$  and the rest. Also, there are other informational based measures for quantum correlations. The linear entropy for the subsystem  $A$  is defined as,

$$\mathcal{T}_t^A = 1 - \text{Tr} \rho_t^{A^2}. \tag{29}$$

The concurrence (Wootters, 1998; Rungta et al., 2001) between the individual systems  $A$  and  $B$  is given as,

$$C_t^{AB} = \sqrt{2(1 - \text{Tr} \rho_t^{A^2})}. \tag{30}$$

The linear entropy, the lowest order approximation of the von Neumann entropy quantifies the mixedness of a quantum state. While  $C_t^{AB}$  quantifies entanglement between the subsystems  $A$  and  $B$ . All the three measures  $S_t^A$ ,  $\mathcal{T}_t^A$ , and  $C_t^{AB}$  vanish for separable states. Since the joint state here is a pure state the mutual information between systems  $A$  and  $B$  is just twice the von

Neumann entropy of the either system. So it is sufficient to discuss only  $S_t^A$  to describe the dynamics. Here, we have taken the system size  $N = 100$  to illustrate our results. Note that the maximum value of von Neumann entropy corresponding to each system is  $S_{\text{max}}^A = \ln 100 \approx 4.6052$  for one particle states.

Fig. 6 show the time dependence of difference between average energies of individual systems ( $\Delta E = E^A - E^B$ ), the average interaction energy divided by twice coupling parameter, i.e.,  $E^{\text{int}}/2\varepsilon$ , between the systems  $A$  and  $B$  and the von Neumann entropy ( $S^A$ ) of the systems  $A$  or  $B$  for different values of  $\varepsilon$  and  $n$ . The initial state we have taken is  $|\psi_0\rangle = |1, N/2\rangle$  and number of qubits in each system  $N = 100$ . The state  $|\psi_0\rangle = |1, N/2\rangle$  means the down spin is at the first site in system  $A$  and in site  $N/2$  in system  $B$ . Since the systems are closed or ring like, the down spins are farthest in this particular initial state and thus most unlikely to couple.

We see that all the three quantities  $\Delta E$ ,  $E^{\text{int}}/2\varepsilon$ , and  $S^A$  are non-monotonic functions of  $\varepsilon$  after certain number of kicks. As shown in Fig.6(a)–(c) the difference between the average energies ( $\Delta E$ ) of the individual systems  $A$  and  $B$  initially grows negative from zero with time, independent of the value  $\varepsilon$  for all values of  $\tau$ . As shown in Fig. 6(a)  $\Delta E$  becomes negative for  $\varepsilon < 0.5$  and slightly positive for  $\varepsilon > 0.5$  after certain value of  $n$ . This means starting from the same initial state with two different values of coupling constant ( $\varepsilon < 0.5$  or,  $\varepsilon > 0.5$ ), results in two completely different energy distributions in the systems  $A$  and  $B$ . For large  $n$  and  $\varepsilon > 0.5$ , the quantity  $\Delta E$  is almost zero for  $\tau = 0.3$  and  $\tau = 0.5$  as shown in Fig. 6(b) and (c) respectively. This indicates that the energies of the individual systems tend to have a common value for  $\varepsilon > 0.5$  and different for  $\varepsilon < 0.5$  for kicking period parameter  $\tau \gtrsim 0.3$ . It is a clear indication of a dynamical phase transition at  $\varepsilon = 0.5$ . So, the quantity  $\Delta E$  may serve as an order parameter for the transition.

Since the systems start from uncoupled state the average interaction energy is zero initially. As time evolves they get coupled and develops nonzero average interaction energy and  $E^{\text{int}}/2\varepsilon$  shows a minimum at  $\varepsilon = 0.5$  for all values  $\tau$ , as shown in Fig. 6(d)–(f). The non-monotonicity begins nearly after  $n = 500$  (equivalently  $t \approx 7.96$ ),  $n = 400$  (equivalently  $t \approx 19.10$ ), and  $n = 300$  (equivalently  $t \approx 23.88$ ) respectively. In contrast, the von Neumann entropy increases from zero and shows a maximum at  $\varepsilon = 0.5$  irrespective of the value of  $\tau$ , as shown in Fig. 6(g)–(i). Which means that maximum decoherence of individual systems and entanglement between two systems occur at  $\varepsilon = 0.5$ . But from the Fig. 6 (a)–(c) we conclude that the minima (maxima) of interaction energy (the von Neumann entropy) does not imply  $\Delta E = 0$  in general. We take  $\tau = 0.3$  as a representative case to illustrate our results in detail.

We take  $\tau = 0.3$  as a representative case to illustrate our results in detail. We have shown the behaviour of the quantities  $E^{\text{int}}$ ,  $E^{\text{int}}/2\varepsilon$ ,  $S^A$ ,  $E^A$ , and  $E^B$  as a function of  $\varepsilon$  after 1000 kicks in Fig. 7. As shown in Fig. 7 (a), (b), and (c) all the three quantities  $E^{\text{int}}$ ,  $E^{\text{int}}/2\varepsilon$ , and  $S^A$  show a non analytic behaviour at  $\varepsilon = 0.5$ —which confirms the transition there. In Fig. 7(d) energies of the individual systems suddenly coincide with each other above  $\varepsilon = 0.5$ . This means the individual systems share

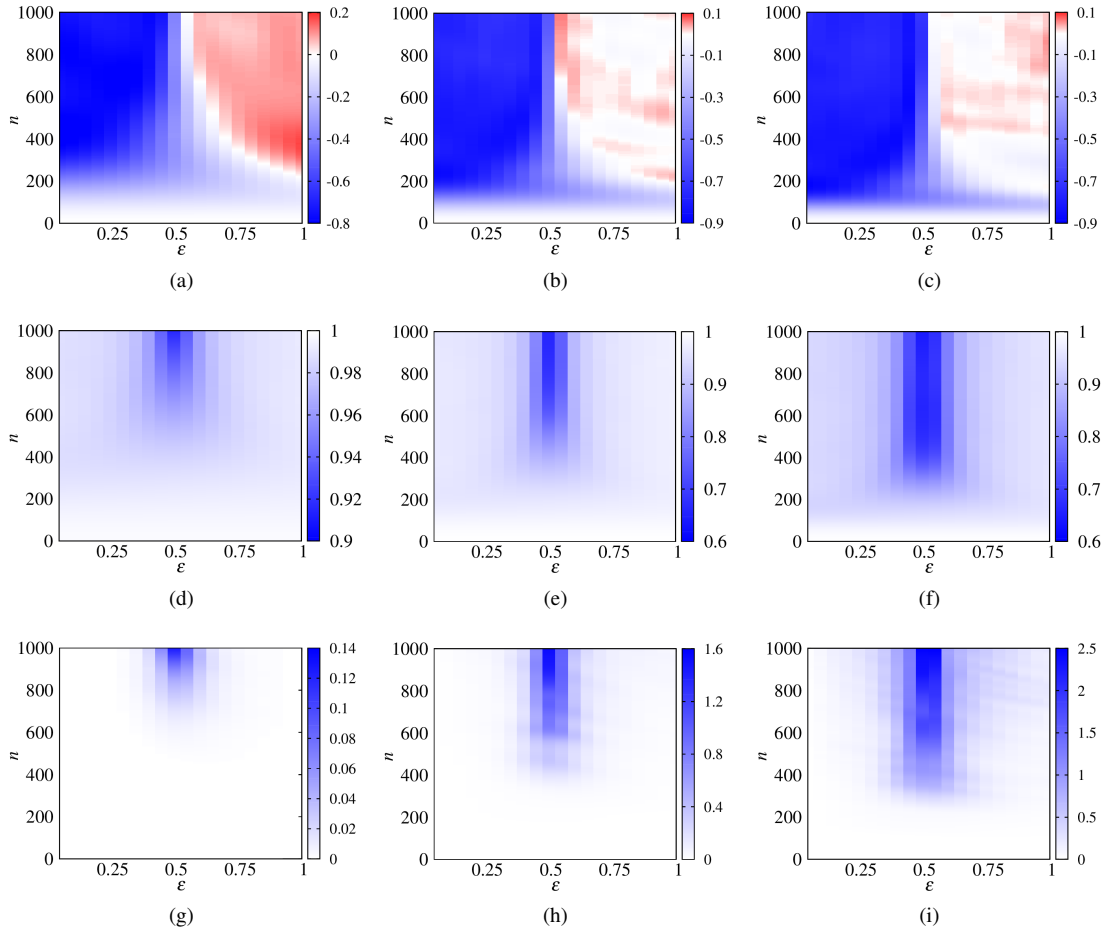


Figure 6: (color online) The difference between the energies of system  $A$  and  $B$  ( $\Delta E = E^A - E^B$ ) as a function of number of kicks ( $n$ ) and the coupling parameter ( $\varepsilon$ ) for kicking intervals (a)  $0.1/2\pi$  (b)  $0.3/2\pi$  (c)  $0.5/2\pi$ . The average interaction energy divided by twice of the coupling parameter ( $E^{\text{int}}/2\varepsilon$ ) as a function of number of kicks ( $n$ ) and the coupling parameter ( $\varepsilon$ ) for kicking intervals (d)  $0.1/2\pi$  (e)  $0.3/2\pi$  (f)  $0.5/2\pi$ . The von Neumann entropy ( $S^A$  or  $S^B$ ) as a function of number of kicks ( $n$ ) and the coupling parameter ( $\varepsilon$ ) for kicking intervals (g)  $0.1/2\pi$  (h)  $0.3/2\pi$  (i)  $0.5/2\pi$ . Number of qubits in each system:  $N = 100$ . Initial state:  $x_0 = 1, y_0 = N/2$ .

their energies equally indicating the quantum synchronization.

#### 4.1. Inter-system single-qubit mutual information

It is also interesting to investigate the correlation between individual qubits in system  $A$  and system  $B$  in order to explain the dynamical phase transition that occurs at  $\varepsilon = 0.5$ . We take  $\tau = 0.3$  as our representative case to show the time dependence of mutual information between  $j_A$  th qubit in system  $A$  and  $j_B$  th qubit in system  $B$  in Fig. 8. Initially, every qubit in each system is uncorrelated. As time evolves they get correlated and the locus of maximally correlated qubits spreads out with time circularly in  $(j_A, j_B)$  plane centering the initial state, i.e.,  $(1, N/2)$ . As shown in Fig. 8 (a), (d), (g), (j) and (c), (f), (i), (l) for  $\varepsilon = 0.05$  and  $\varepsilon = 1.00$  respectively, after a certain time it stops growing due to the convex light cone structure of the Green function (Sur and Subrahmanyam, 2019). Even after a long time maximally correlated pairs reside inside a circle centering the point  $(1, N/2)$  for  $\varepsilon = 0.05$  and  $\varepsilon = 1.0$  as shown in Fig. 8 (j) and (l) respectively. In contrast, for  $\varepsilon = 0.5$  this locus no longer remains circular after a certain time and spreads in the

$(j_A, j_B)$  plane as shown in Fig. 8 (h) and (k). Hence, the spreading of quantum correlation is a signature for the transition. Not only the mutual information (twice of  $S^A$ ) between the systems  $A$  and  $B$  is maximum at  $\varepsilon = 0.5$  as seen from Fig. 7(c) but also maximum value of the mutual information between individual qubits is also much higher. As seen from Fig. 8 (j), (k), and (l) the maximum value of mutual information is 0.00025 for  $\varepsilon = 0.05$ , is 0.01 for  $\varepsilon = 0.5$ , and is 0.0016 for  $\varepsilon = 1.0$  respectively.

#### 4.2. A discussion on Local coupling

In this context we want to discuss another type of coupling scheme. The coupling discussed above is global in the sense that every qubit in system  $A$  interacts with every qubit in system  $B$ . Instead the coupling can be local; the limiting case would be the coupling occurs between the two systems  $A$  and  $B$  only through individual qubits. In this scheme the  $j^{\text{th}}$  spin in system  $A$  will get coupled only with the  $j^{\text{th}}$  spin in system  $B$  via the same time and space dependent potential. For further mention this will be named as ‘local coupling’. The coupling Hamil-



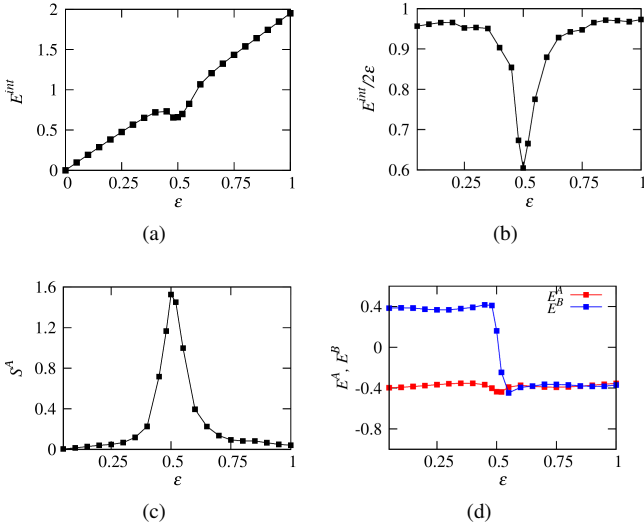


Figure 7: (color online) (a) The average interaction energy ( $E^{\text{int}}$ ), (b) the average interaction energy divided by twice the coupling constant ( $E^{\text{int}}/2\epsilon$ ), (c) the von Neumann entropy ( $S^A$ ), (d) the average individual energies  $E^A$  and  $E^B$  as a function of the coupling constant  $\epsilon$  after 1000 kicks per kicking period parameter  $\tau = 0.3$ .

tonian can be obtained from Eq. 9 by introducing a Kronecker delta function and is given by,

$$H^{AB}(t) = \frac{\epsilon}{2} \sum_{j_A, j_B=1}^N \delta_{j_A, j_B} \cos\left(\frac{2\pi j_A}{N}\right) \cos\left(\frac{2\pi j_B}{N}\right) \sigma_{j_A}^z \sigma_{j_B}^z \sum_{n=-\infty}^{\infty} \delta\left(\frac{2\pi t}{\tau} - n\right). \quad (31)$$

This type of coupling has no ‘classical’ analog; in the sense that the coupling Hamiltonian cannot be factorized in two parts corresponding to systems  $A$  and  $B$  as given in Eq. 8. The joint state of system  $A$  and  $B$  is still given by Eq. 24, but the wave function of the joint state after  $n$  kicks will be given by,

$$\tilde{G}_{x_0, y_0}^{x_n, y_n}(n) = \sum_{x_1, x_2, \dots, x_{n-1}} \sum_{y_1, y_2, \dots, y_{n-1}} \prod_{i=0}^{n-1} G_{x_i}^{x_{i+1}}\left(\frac{\tau}{2\pi}\right) G_{y_i}^{y_{i+1}}\left(\frac{\tau}{2\pi}\right) \times e^{i(g + \epsilon(1 - \delta_{x_{i+1}, y_{i+1}}))(\cos(\frac{2\pi x_{i+1}}{N}) + \cos(\frac{2\pi y_{i+1}}{N}))}. \quad (32)$$

As seen in the above equation the joint Green function behaves like two uncoupled systems with an effective site dependent potential strength parameter  $g + \epsilon(1 - \delta_{x_{i+1}, y_{i+1}})$ . This makes the joint Green function very different from the same given in Eq. 24. Here, the interaction energy after  $n$  kicks is given by,

$$E_n^{\text{int}} = \epsilon \frac{N}{4} - \epsilon \sum_{x_n, y_n} |\tilde{G}_{x_0, y_0}^{x_n, y_n}(n)|^2 \left( \cos\left(\frac{2\pi x_n}{N}\right) + \cos\left(\frac{2\pi y_n}{N}\right) \right) (1 - \delta_{x_n, y_n}). \quad (33)$$

Fig. 9 show the time dependence of difference between average energies of individual systems ( $\Delta E = E^A - E^B$ ), average

interaction energy divided by the coupling parameter ( $E^{\text{int}}/\epsilon$ ) between the systems  $A$  and  $B$  and von Neumann entropy ( $S^A$ ) of the systems  $A$  or  $B$  for different values of  $\epsilon$  and  $n$  for the ‘local coupling’ scheme. Here, the initial state plays a significant role in the dynamics because the interaction is local. If the down spin in system  $A$  is very far from the same in system  $B$  the systems will have effectively no coupling. Hence, unlike the earlier case we choose the initial state  $|1, N/5\rangle$  to show our results. However, we have tried with other initial states but the dynamics is not qualitatively very different.

As shown in Fig. 9(a)–(c), the difference between the average energies of the individuals systems ( $\Delta E$ ) initially decreases with time independent of the value of  $\epsilon$  and  $\tau$ , and mostly remain so. Unlike the earlier coupling scheme here no such branching of  $\Delta E$  depending on the coupling is observed. Same kind of trend is seen in in case of  $E^{\text{int}}/\epsilon$ , as shown in Fig. 9(d)–(f). Fig. 9(g)–(i) show the von Neumann entropy ( $S^A$ ) is very small compared to the earlier case. This means the coupling is negligible or in other words, the do not get entangled appreciably. Only thing we can say that  $S^A$  increases with kicking period.

## 5. Conclusions

In conclusion, we have studied the synchronization for coupled Harper systems. We extended the concept of synchronization from classical to quantum scenario for the same coupled systems. To do so, we have investigated through the method of average interaction energy between the participating subsystems in both classical and quantum cases. Further, we have followed different paths also to study the synchronization.

In this paper, to make the analogy between the classical and the quantum scenarios, we have illustrated our results explicitly for  $\tau = 0.3$  for the classical part. In Fig. 1, 2, 3, 4, and 5 all plots are done using a single set of initial conditions ( $x^A(0), p^A(0), x^B(0), p^B(0)$ ) = (0.5, 0.4, 0.3, 0.5). However, one may obtain unaltered conclusions with other set of initial conditions. Here, we adopt the joint probability density technique, in addition to the average interaction energy method, to detect the synchronized (desynchronized) state. But, choosing of different  $\tau$  may not lead to observe the transition between the synchronized and the desynchronized states, though there is a kink observed in the average interaction energy. For example, at  $\tau = 0.1$ , the discontinuity is observed at  $\epsilon = 0.5$  (see Fig. 4(a) or (b)), but the difference in the joint probability density does not confirm this transition (see Fig. 4(c) and (d)). Similar kind of observations one can get for any  $\tau \lesssim 0.3$ . Further, for  $\tau \gtrsim 0.5$ , since the intrinsic subsystems show the global chaotic nature and they are always in synchronized state independent of the coupling strength. This leads to make us the possible conclusion that *the transition is always associated with the kink, but the converse is not always true*. Further, one possible future direction may be the explicit study of the dynamics of the coupled subsystems in the desynchronized state, which seems to us the existence of local chaos (Walker and Ford, 1969). However, in the synchronized state, the participating subsystems are full fledged chaotic in nature.

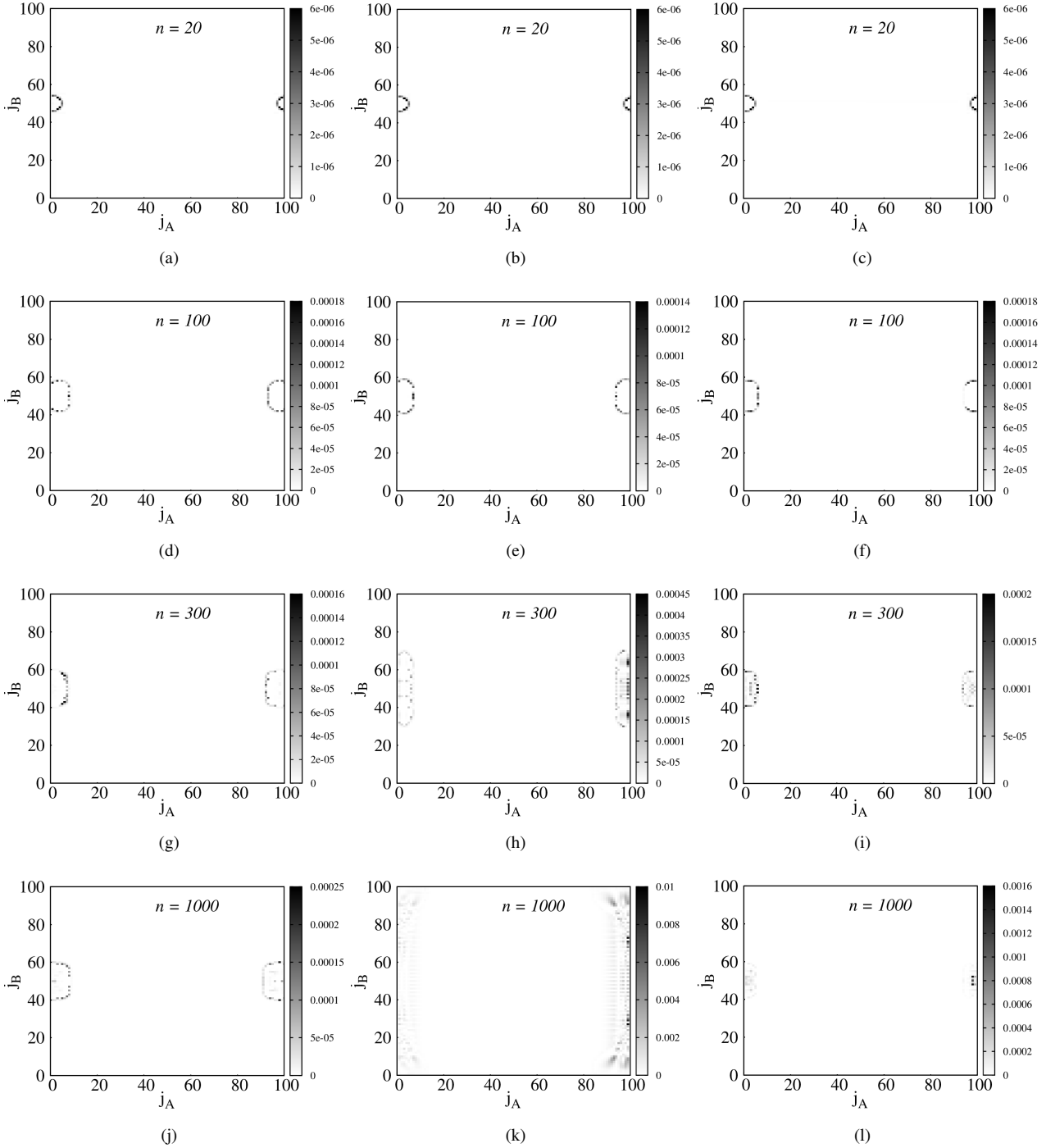


Figure 8: The mutual information between  $j_A^{\text{th}}$  qubit in system A and  $j_B^{\text{th}}$  qubit in system B for different coupling strength ( $\varepsilon$ ) and time ( $n$ ): (a)  $\varepsilon = 0.05$ ,  $n = 20$ , (b)  $\varepsilon = 0.50$ ,  $n = 20$ , (c)  $\varepsilon = 1.00$ ,  $n = 20$ , (d)  $\varepsilon = 0.05$ ,  $n = 100$ , (e)  $\varepsilon = 0.50$ ,  $n = 100$ , (f)  $\varepsilon = 1.00$ ,  $n = 100$ , (g)  $\varepsilon = 0.05$ ,  $n = 300$ , (h)  $\varepsilon = 0.50$ ,  $n = 300$ , (i)  $\varepsilon = 1.00$ ,  $n = 300$ , (j)  $\varepsilon = 0.05$ ,  $n = 1000$ , (k)  $\varepsilon = 0.50$ ,  $n = 1000$ , (l)  $\varepsilon = 1.00$ ,  $n = 1000$ . In all subplots, the abscissa denotes the actual position of the  $j_A^{\text{th}}$  qubit in system A and the ordinate denotes the actual position of the  $j_B^{\text{th}}$  qubit in system B. Initial state:  $x_0 = 1$ ,  $y_0 = N/2$ . Kicking interval parameter:  $\tau = 0.3$ .

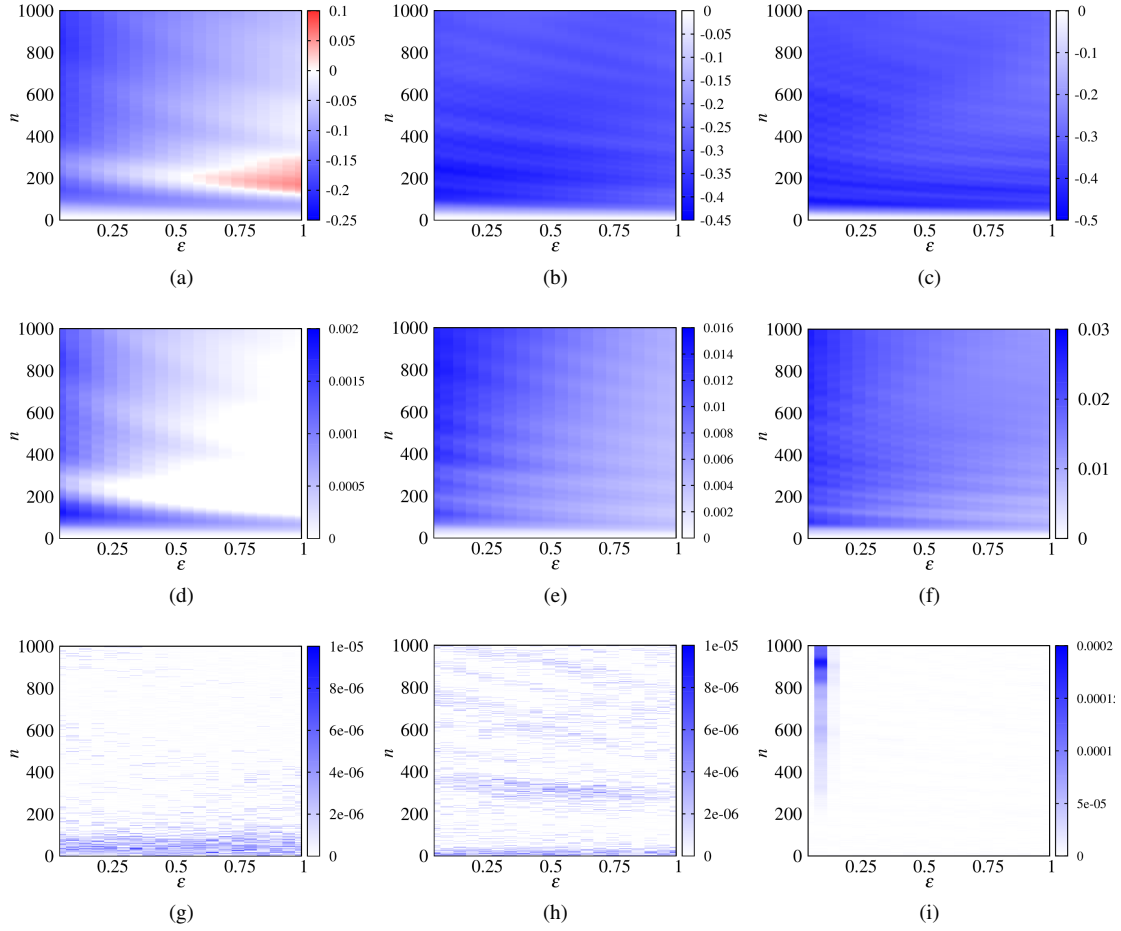


Figure 9: (*color online*) Local coupling scheme: The difference between the energies of system  $A$  and  $B$  ( $\Delta E = E^A - E^B$ ) as a function of number of kicks ( $n$ ) and the coupling parameter ( $\varepsilon$ ) for kicking intervals (a)  $0.1/2\pi$  (b)  $0.3/2\pi$  (c)  $0.5/2\pi$ . The average interaction energy divided by the coupling parameter ( $E^{\text{int}}/\varepsilon$ ) as a function of number of kicks ( $n$ ) and the coupling parameter ( $\varepsilon$ ) for kicking intervals (d)  $0.1/2\pi$  (e)  $0.3/2\pi$  (f)  $0.5/2\pi$ . The von Neumann entropy ( $S^A$  or  $S^B$ ) as a function of number of kicks ( $n$ ) and the coupling parameter ( $\varepsilon$ ) for kicking intervals (g)  $0.1/2\pi$  (h)  $0.3/2\pi$  (i)  $0.5/2\pi$ . Number of qubits in each system:  $N = 100$ . Initial state:  $x_0 = 1, y_0 = N/5$ .

In quantum scenario, we observe a dynamical phase transition at  $\varepsilon = 0.5$  irrespective of the kicking period. Where,  $\varepsilon = 0.5$  is the transition point from desynchronized state to MS state in classical context for  $\tau \gtrsim 0.3$ . In this regime two quantum systems  $A$  and  $B$  equal their energies by sharing though the coupling for  $\varepsilon > 0.5$ . For the case  $\tau \lesssim 0.3$  the quantum systems instead show a energy level crossing at  $\varepsilon = 0.5$ . We do not see any transition in the classical context also as mentioned already. The average interaction energy between the systems  $A$  and  $B$  divided by the coupling constant  $\varepsilon$  shows a minimum at  $\varepsilon = 0.5$  irrespective of the kicking period. This is a common feature which is seen in both classical and quantum scenario. Moreover, the quantum correlation measures, viz., the von Neumann entropy shows a maximum at  $\varepsilon = 0.5$ . So, the transition is associated with a much larger value of entanglement between the systems  $A$  and  $B$ , or in other words, more decoherence in the individual systems. So, the transition from desynchronized to synchronized state can be thought of as a classical manifestation of a dynamical phase transition in quantum many body system. A small discussion on inter system single qubit correlation is given in Section 4.1. It can be seen that quantum correlations spread over the systems at the transition point.

We studied the quantum scenario and discussed the results in joint Green function formalism, i.e., starting from one down spin(or, one magnon) in each system. Since, system is non interacting, the time-dependent wave function from any initial state can be written as a product of the joint Green function. Although a state with more number of down spins in each system will result in much stronger coupling the qualitative features of our results will not change.

We have not commented about the nature of the transition in both classical and quantum scenarios. Though we have analytical expressions for the time dependent wave functions, energies, etc., in quantum dynamics—we need to check the analyticities of the energies, entropies or other correlations at the transition point. Hence determining the nature of the transition is a challenging analytical problem.

Finally, the local coupling scheme which we have discussed does not give rise to any such transitions. The possible reasons might be the coupling has no classical analog, i.e., the coupling Hamiltonian cannot be written as a product of two terms corresponding to the systems  $A$  and  $B$  and the coupling is very weak. It seems that the transition is a ‘classical’ phenomena, which cannot be obtained through local coupling. This requires further investigation.

## Acknowledgements

The authors thank S. Chakraborty, A. Lakshminarayan, V. Subrahmanyam, and H. Wanare for fruitful discussions. S.S. acknowledges the financial support from CSIR, India.

## References

## References

Aguiar, M., Ashwin, P., Dias, A., Field, M., 2011. Dynamics of coupled cell networks: Synchrony, heteroclinic cycles and inflation. *J. Nonlin. Sci.*

- 21 (2), 271.
- Artuso, R., Borgonovi, F., Guarneri, I., Rebuzzini, L., Casati, G., Dec 1992. Phase diagram in the kicked harper model. *Phys. Rev. Lett.* 69, 3302–3305.
- Artuso, R., Casati, G., Borgonovi, F., Rebuzzini, L., Guarneri, I., 1994. Fractal and dynamical properties of the kicked Harper model. *Int. J. Mod. Phys. B* 08 (03), 207–235.
- Basu, C., Mookerjee, A., Sen, A. K., Thakur, P. K., aug 1991. Metal-insulator transition in one-dimensional quasi-periodic systems. *J. Phys. Condens. Matter* 3 (32), 6041–6053.
- Bemani, F., Motazedifard, A., Roknizadeh, R., Naderi, M. H., Vitali, D., Aug 2017. Synchronization dynamics of two nanomechanical membranes within a fabry-perot cavity. *Phys. Rev. A* 96, 023805.
- Bethe, H., 1931. Zur theorie der metalle. *Z. Phys.* 71, 205–226.
- Blasius, B., Huppert, A., Stone, L., May 1999. Complex dynamics and phase synchronization in spatially extended ecological systems. *Nature* 399 (6734), 354.
- Boccaletti, S., Kurths, J., Osipov, G., Valladares, D. L., Zhou, C. S., 2002. The synchronization of chaotic systems. *Phys. Rep.* 366 (1-2), 1.
- Bose, S., Nov 2003. Quantum communication through an unmodulated spin chain. *Phys. Rev. Lett.* 91, 207901.
- Christandl, M., Datta, N., Ekert, A., Landahl, A. J., Sept 2004. Perfect state transfer in quantum spin networks. *Phys. Rev. Lett.* 92, 187902.
- Einstein, A., Podolsky, B., Rosen, P., May 1935. Can quantum-mechanical description of physical reality be considered complete? *Phys. Rev.* 47, 777.
- Ghosh, A., Godara, P., Chakraborty, S., 2018a. Understanding transient uncoupling induced synchronization through modified dynamic coupling. *Chaos* 28 (5), 053112.
- Ghosh, A., Shah, T., Chakraborty, S., 2018b. Occasional uncoupling overcomes measure desynchronization. *Chaos* 28 (12), 123113.
- Gupta, S., De, S., Janaki, M. S., Iyengar, A. N. S., 2017. Exploring the route to measure synchronization in non-linearly coupled Hamiltonian systems. *Chaos* 27 (11), 113103.
- Hampton, A., Zanette, D. H., Sep 1999. Measure synchronization in coupled Hamiltonian systems. *Phys. Rev. Lett.* 83, 2179–2182.
- Harper, P. G., oct 1955. The general motion of conduction electrons in a uniform magnetic field, with application to the diamagnetism of metals. *Proc. Phys. Soc.*, A 68 (10), 879–892.
- Huygens, C., 1673. *Horoloqium oscilatorium*. Apud F. Muquet, Parisiis.
- Iomin, A., Fishman, S., Aug 1998. Driven electrons on the fermi surface. *Phys. Rev. Lett.* 81, 1921–1924.
- Iomin, A., Fishman, S., Jan 2000. Model for a metal-insulator transition in antidot arrays induced by an external driving field. *Phys. Rev. B* 61, 2085–2089.
- Lakshminarayan, A., Aug 2001. Entangling power of quantized chaotic systems. *Phys. Rev. E* 64, 036207.
- Lakshminarayan, A., Subrahmanyam, V., May 2003. Entanglement sharing in one-particle states. *Phys. Rev. A* 67, 052304.
- Lieb, E., Schultz, T., Mattis, D., 1961. Two soluble models of an antiferromagnetic chain. *Annals of Physics* 16 (3), 407 – 466.
- Lima, R., Shepelyansky, D., Sep 1991. Fast delocalization in a model of quantum kicked rotator. *Phys. Rev. Lett.* 67, 1377–1380.
- Miller, P. A., Sarkar, S., Aug 1999. Signatures of chaos in the entanglement of two coupled quantum kicked tops. *Phys. Rev. E* 60, 1542–1550.
- Pecora, L. M., Carroll, T. L., Feb. 1990. Synchronization in chaotic systems. *Phys. Rev. Lett.* 64, 821.
- Pecora, L. M., Carroll, T. L., 2015. Synchronization of chaotic systems. *Chaos* 25 (9), 097611.
- Pikovsky, A., Rosenblum, M., Kurths, J., 2001. *Synchronization*. Cambridge University Press, New York.
- Porat-Shliom, N., Chen, Y., Tora, M., Shitara, A., Masedunskas, A., Weigert, R., oct 2014. In vivo tissue-wide synchronization of mitochondrial metabolic oscillations. *Cell Reports* 9, 514–521.
- Qiu, H., Juliá-Díaz, B., Garcia-March, M. A., Polls, A., Sep 2014. Measure synchronization in quantum many-body systems. *Phys. Rev. A* 90, 033603.
- Qiu, H., Tian, J., Fu, L.-B., Apr 2010. Collective dynamics of two-species bose-einstein-condensate mixtures in a double-well potential. *Phys. Rev. A* 81, 043613.
- Qiu, H., Zambrini, R., Polls, A., Martorell, J., Juliá-Díaz, B., Oct 2015. Hybrid synchronization in coupled ultracold atomic gases. *Phys. Rev. A* 92, 043619.
- Roulet, A., Bruder, C., Aug 2018. Quantum synchronization and entanglement generation. *Phys. Rev. Lett.* 121, 063601.

- Rungta, P., Bužek, V., Caves, C. M., Hillery, M., Milburn, G. J., Sep 2001. Universal state inversion and concurrence in arbitrary dimensions. *Phys. Rev. A* 64, 042315.
- Saxena, G., Prasad, A., Ramaswamy, R., May 2013. Amplitude death phenomena in delay-coupled hamiltonian systems. *Phys. Rev. E* 87, 052912.
- Subrahmanyam, V., Mar 2004. Entanglement dynamics and quantum-state transport in spin chains. *Phys. Rev. A* 69, 034304.
- Sur, S., Subrahmanyam, V., 2017. Remotely detecting the signal of a local decohering process in spin chains. *J. Phys. A* 50 (20), 205303.
- Sur, S., Subrahmanyam, V., 2019. Loschmidt echo of local dynamical processes in integrable and non integrable spin chains. *J. Phys. A* (accepted).
- Tian, J., Qiu, H., Wang, G., Chen, Y., Fu, L.-b., Sep 2013a. Measure synchronization in a two-species bosonic josephson junction. *Phys. Rev. E* 88, 032906.
- Tian, J., Qiu, H., Wang, G., Chen, Y., Fu, L.-b., Sep 2013b. Measure synchronization in a two-species bosonic josephson junction. *Phys. Rev. E* 88, 032906.
- Vincent, U. E., 2005. Measure synchronization in coupled Duffing Hamiltonian systems. *New J. Phys.* 7 (1), 209.
- Walker, G. H., Ford, J., Dec 1969. Amplitude instability and ergodic behavior for conservative nonlinear oscillator systems. *Phys. Rev.* 188, 416–432.
- Wang, X., Li, H., Hu, K., Hu, G., 2002. Partial measure synchronization in Hamiltonian systems. *Int. J. Bifurc. Chaos* 12 (05), 1141–1148.
- Wang, X., Zhan, M., Lai, C.-H., Gang, H., Jun 2003. Measure synchronization in coupled  $\varphi^4$  Hamiltonian systems. *Phys. Rev. E* 67, 066215.
- Wootters, W. K., March 1998. Entanglement of formation of an arbitrary state of two qubits. *Phys. Rev. Lett.* 80, 2245.